This is the final accepted version of the manuscript published in
Physical Review A, Vol. 96, Issue 2, Paper 023404, (2017)
DOI.: https://doi.org/10.1103/PhysRevA.96.023404

Ionic Dynamics Underlying Strong Field Dissociative Molecular Ionization

Arthur Zhao,[1] Péter Sándor,[2] Vincent Tagliamonti,[1] Tamás Rozgonyi,[3], Philipp Marquetand,[4] and Thomas Weinacht[1]

[1]*Department of Physics and Astronomy, Stony Brook University, Stony Brook NY 11794-3800*

[2]*Department of Physics, University of Virginia, Charlottesville VA 22904*

[3]*Institute of Materials and Environmental Chemistry, Research Centre for Natural Sciences, Hungarian Academy of Sciences, Budapest 1117 Magyar tudósok krt. 2, Hungary and*

[4]*University of Vienna, Faculty of Chemistry, Institute of Theoretical Chemistry, Währinger Str. 17, 1090 Wien, Austria*

(Dated: July 5, 2017)

Abstract

We study strong field molecular ionization, with a focus on indirect ionization to dissociative excited ionic states. Indirect ionization, also known as post-ionization excitation, refers to the excitation of the molecular cation following ionization to a lower lying state. We propose two possible mechanisms underlying indirect ionization – resonant transitions facilitated by nuclear dynamics and non-adiabatic transitions driven by the laser field off resonance. We compare them by measuring the dependence of the indirect ionization yield on pulse duration for cations with different electronic structures. Both experiments and simulations confirm the importance of nuclear dynamics in indirect ionization and indicate the presence of off-resonant non-adiabatic transitions.

I. INTRODUCTION

Strong field ionization (SFI) has been of significant interest since it provides access to attosecond electron dynamics via high harmonic generation and allows for direct probing of excited state molecular dynamics on ultrafast timescales [1–4]. While most work considers ionization to the ground state of the molecular cation, there have also been several observations of ionization to excited ionic states in SFI [5–15]. In this work, we consider two mechanisms underlying ionization to excited states, and compare their relative importance in different parameter regimes.

In a recent work [12], we demonstrated that there are two pathways to populate an excited ionic state - (1) Direct ionization, in which the neutral molecule is directly ionized to an excited ionic state, corresponding to the removal of an inner orbital electron; (2) Indirect ionization (also known as post-ionization excitation), in which the molecule is first ionized to the ground (or a low-lying) ionic state and then excited by the field to a high-lying state. If the initial ionic state is non-dissociative while the final state is dissociative, then these two pathways can be separated by coincidence measurements. In coincidence measurements, a photoelectron is detected together with its partner photoion. At the moment of ionization, an electron is liberated with the amount of kinetic energy (KE) given by

$$\mathrm{KE} = \mathrm{n}\hbar\omega - \mathrm{I}_\mathrm{S}^\mathrm{i} - \mathrm{U} \tag{1}$$

where n is the number of photons absorbed, $\mathrm{I}_\mathrm{S}^\mathrm{i}$ is the Stark shifted ionization potential to the i^{th} excited state, and U is the ponderomotive potential. Given this, we can infer the state of the ion by measuring the photoelectron kinetic energy. However, after ionization, the ion is still subject to the laser field and can potentially undergo transitions between different states. For instance, it can be promoted to a dissociative state and produce fragments. Therefore, ion detection, together with knowledge of the fragmentation channels, provides us with information on the final ionic state.

We consider two mechanisms that can drive indirect ionization, illustrated by the cartoons in Figure 1. The first one is a resonant transition between electronic states of the cation driven by the laser and facilitated by nuclear dynamics. Panel (a) of Figure 1 illustrates such a situation: the molecule is first ionized to the ground ionic state D_0 at the Franck-Condon point (FC), then as the wave packet evolves along the potential surface, it reaches a one-photon resonance where it's excited to an upper state D_N. Since it usually involves

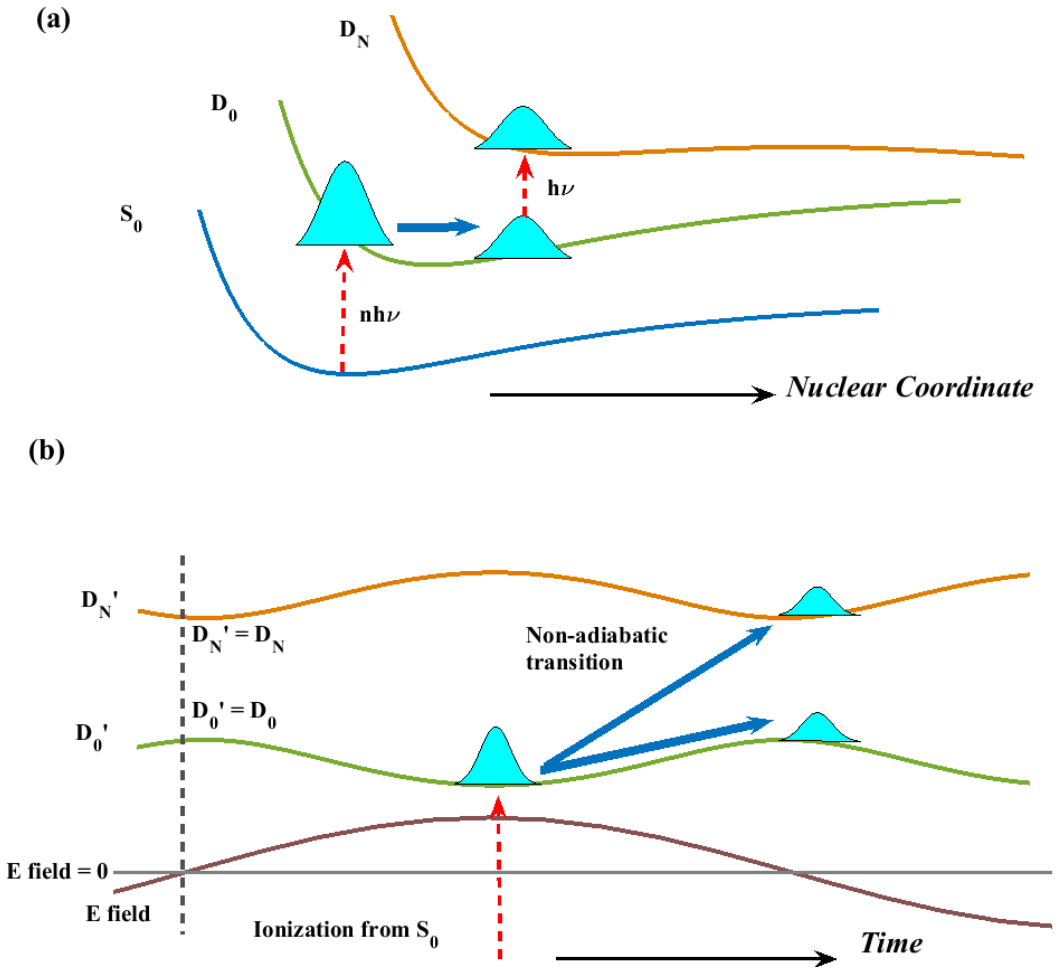

FIG. 1. Cartoon illustration of two possible indirect ionization mechanism: (a) nuclear dynamics induced resonant transition. After ionization, the nuclear wavepacket starts evolving along the potential curve away from the Franck-Condon (FC) point toward the minimum of the potential (MIN). A transition to a high-lying ionic states can occur if a resonance condition is met. (b) Non-adiabatic transition. After tunnel ionization near the peak of the field, a non-adiabatic shut off of the laser field induces a "hopping" between two *dressed* states. This is most likely to happen when the laser field crosses zero. Note the x-axes in two panels are different.

nuclear motion (which takes some time) to reach a resonance, we expect this mechanism to be sensitive to pulse duration.

The second mechanism is via an off-resonance non-adiabatic transition induced by the laser field (in contrast to non-adiabaticity resulting from the breakdown of the Born-Oppenheimer approximation) [16]. We call the eigenstates of the field-free Hamiltonian

the *bare* (diabatic) states, denoted by $\mathrm{D_N}, \mathrm{N} = 0, 1, 2...$, and those of the *total* Hamiltonian (molecule + field) *dressed* (adiabatic) states, denoted by $\mathrm{D'_N}, \mathrm{N} = 0, 1, 2....$ We discuss this mechanism in the *dressed* basis since we expect it to be important when the field is strong and the bare states do not provide a good description of the instantaneous eigenstates in the field. This expectation is confirmed by the derivations given below.

Panel (b) of Figure 1 shows a simple case of tunnel ionization at the peak of a laser pulse, leaving the cation in the lowest *dressed* ionic state $\mathrm{D'_0}$. We assume the tunneling takes places instantaneously since we are only concerned with what happens afterwards. This dressed state can be expressed as a linear combination of *bare* eigenstates, $\mathrm{D'_0} = a\mathrm{D_0} + b\mathrm{D_N},\ |a|^2 + |b|^2 = 1$. If the field were turned off very slowly, then this state would evolve adiabatically to the ground state of the bare Hamiltonian, $\mathrm{D_0}$. However, if the field turns off so rapidly that there is no time for any population transfer (sudden approximation), then the molecule is projected onto the bare states such that we find a probability of $|a|^2$ being in $\mathrm{D_0}$ and $|b|^2$ in $\mathrm{D_1}$ after the pulse. Generally speaking, as the field varies in time, the diagonalization of the *total* Hamiltonian is time-dependent and its eigenvectors experience a rotation in the Hilbert space. This rotation introduces a coupling among the *dressed* states, since the time derivative of one state has a non-zero projection onto other states. The faster the field varies, and the smaller the energy gaps among the dressed states are, the larger the rate of non-adiabatic transitions. These non-adiabatic transitions manifest themselves as indirect ionization, since they take place after the initial ionization, but still in the presence of the laser field.

In order to illustrate the differences between these two mechanisms, we consider the time-dependent Schrödinger equation (TDSE) for a two-level system coupled to an external field via dipole coupling. In the *bare* basis, i.e., field-free basis, and assuming constant potential energies E_a and E_b (i.e. fixed nuclei), the TDSE can be written in the matrix form as

$$i\hbar\frac{\mathrm{d}}{\mathrm{d}t}\begin{pmatrix} a(t)e^{-i\omega_a t} \\ b(t)e^{-i\omega_b t} \end{pmatrix} = \begin{pmatrix} E_a & V(t) \\ V(t)^* & E_b \end{pmatrix}\begin{pmatrix} a(t)e^{-i\omega_a t} \\ b(t)e^{-i\omega_b t} \end{pmatrix} \tag{2}$$

where $E_a = \hbar\omega_a$, $E_b = \hbar\omega_b$ and $|a(t)|^2 + |b(t)|^2 = 1$. We assume the field is near resonance (small detuning, $\Delta = \omega - (\omega_b - \omega_a) << \omega$), and ignore the matrix elements related to the nuclear kinetic energy. For simplicity, we also assume a real coupling $V(t) = -\mu\epsilon(t)\cos(\omega t) = V(t)^*$, where μ is the transition dipole moment, $\epsilon(t)$ is the pulse envelope and ω is the carrier

frequency. Under these conditions we can apply the rotating wave approximation (RWA) to Eq. 2 and arrive at

$$\begin{cases} \dot{a}(t) = \frac{i\chi(t)}{2} e^{+i\Delta t} b(t) \\ \dot{b}(t) = \frac{i\chi(t)}{2} e^{-i\Delta t} a(t) \end{cases} \tag{3}$$

where $\chi(t) = \mu\epsilon(t)/\hbar$ is the Rabi frequency. The coupling consists of an amplitude ($\sim \chi(t)$) and a phase ($\sim \Delta t$). It's instructive to look at the perturbative behavior of Equation 3 when the transition probability is small, that is, assuming $a(t) \approx 1$ for all $0 \leq t \leq t_0$.

$$b(t_0) \approx \frac{i}{2} \int_0^{t=t_0} \chi(t) e^{-i\Delta t} \mathrm{d}t \tag{4}$$

We note that if Δ is small, then only a moderate $\chi(t)$ is needed to produce significant population transfer since population can build up coherently over time, adding in phase for a time equal to $1/\Delta$. While equation 4 is a perturbative result, one can solve Equation 3 analytically to obtain Rabi oscillations. With an initial condition $|a(0)|^2 = 1$ and $|b(0)|^2 = 0$, we get:

$$\begin{cases} |a(t)|^2 = (\frac{\Delta}{\Omega})^2 + (\frac{\chi}{\Omega})^2 \cos^2(\frac{\Omega t}{2}) \\ |b(t)|^2 = (\frac{\chi}{\Omega})^2 \sin^2(\frac{\Omega t}{2}) \end{cases} \tag{5}$$

We see that the population cycles between two states at the frequency of $\Omega/4$, where $\Omega = \sqrt{\chi^2 + \Delta^2}$. In the case of $\Delta = 0$, $\Omega = \chi$ and a pulse of duration $t = \pi/\chi$, all population is transferred from one state to the other. Such a pulse is termed a π-pulse. Even though nuclear dynamics are not included in the derivation here and we have assumed constant E_a and E_b, some nuclear motion is generally required in order to reach a resonance condition. In other words, Δ generally depends on time indirectly via nuclear dynamics.

The above solution is derived in the limit of moderate Rabi frequency and small detuning. Now we consider the case of non-adiabatic transitions, which take place in the limit of large Rabi frequency. Note that there is no constraint on the detuning here, and hence no RWA. Since the field is strong and the Stark shifts are significant, it's better to work in the *dressed* state basis. Let $U(t)$ be the unitary transformation that diagonalizes the instantaneous Hamiltonian $H(t)$:

$$U^{-1}(t) H(t) U(t) = D(t) = \begin{pmatrix} E'_a & 0 \\ 0 & E'_b \end{pmatrix} \tag{6}$$

$$\Psi' = U^{-1}\Psi = \begin{pmatrix} a'(t)e^{-i\omega'_a t} \\ b'(t)e^{-i\omega'_b t} \end{pmatrix} \tag{7}$$

The explicit definition of U is given in Appendix A. We have used a prime to label the equivalent *dressed* state quantities. The TDSE simplifies to:

$$\begin{cases} \dot{a}'(t) = +\frac{\dot{\theta}}{2}\, e^{+iEt/\hbar}\, b'(t) \\ \dot{b}'(t) = -\frac{\dot{\theta}}{2}\, e^{-iEt/\hbar}\, a'(t) \end{cases} \tag{8}$$

$$\dot{\theta} = \frac{2\dot{V}E}{4V^2 + E^2}\ , \qquad E = E_a - E_b \tag{9}$$

As above, we examine the perturbative limit corresponding to $a'(t) \approx 1$:

$$b'(t_0) \approx -\frac{1}{2}\int_0^{t=t_0} \dot{\theta} e^{-iEt/\hbar} \mathrm{d}t \tag{10}$$

Despite the structural similarities between Equations 4 and 10 (or Equation 3 and 8), they have different physical interpretations. The phase of the coupling ($\sim Et/\hbar = (\omega_a - \omega_b)t$) now depends on the energy gap between the two *bare* states, and the amplitude of the coupling ($\sim \dot{\theta}$) depends on the molecule and laser field parameters in a more complicated manner. We note the following: (1) the coupling between states is proportional to the time derivative of the molecule-field coupling, V(t) - i.e., non-adiabaticity is important for strong fields which vary rapidly. The coupling amplitude is maximum when the instantaneous field crosses zero. However, note that due to the phase term, the population change is not necessarily maximal at zero field. In fact, at zero field, the population in one state could be increasing or decreasing, depending on whether the relative phase is constructive or destructive (this is illustrated below in Figure 6). (2) The energy difference between the states influences both the coupling amplitude and the phase evolution. For an energy gap E much larger than V, this coupling amplitude is suppressed as $1/E$. A smaller energy gap minimizes the phase evolution, and hence there is more constructive interference and population transfer. (3) The detuning Δ no longer plays a significant role - hence this mechanism doesn't require a resonance condition which usually involves nuclear dynamics. (4) Population transfer now takes place on a sub-cycle timescale, since $\dot{V}$ contains the carrier frequency.

We've used the *bare state* representation to solve the TDSE in the case of resonant transition, and the *dressed state* representation in the case of non-adiabatic transition. This

gives us a similar set of solutions (4 and 10) for easy comparison. In addition, it suggests that the two mechanisms are important in different coupling regimes – resonant transition requires a small detuning but can otherwise occur with a moderate Rabi frequency, while non-adiabatic transitions require a large Rabi frequency.

Now a natural question arises since these two seemingly different mechanisms originate from the same coupling term in the Hamiltonian - are they really separate effects, or different manifestations of the same effect? In order to answer this question, we go back to the TDSE in the *dressed* state basis, applying Eq. 6 and 7 to $i\hbar\frac{\partial}{\partial t}\Psi(t) = H(t)\Psi(t)$:

$$i\hbar\frac{\partial}{\partial t}\Psi'(t) = D(t)\Psi'(t) - i\hbar U^{-1}(t)\frac{\partial U(t)}{\partial t}\Psi'(t) \tag{11}$$

Since $D(t)$ is diagonal, the second term is the only coupling among states. When $U^{-1}\frac{\partial U}{\partial t}$ *is small*, we can neglect this term, which is equivalent to the adiabatic approximation, that is, all population remains in the same adiabatic (dressed) states through time. On the contrary, when this term is *not* negligible, we have non-adiabatic transitions, Eq.8. Now how do resonant transitions enter this equation? It must be contained in the second term as well, since there is no other coupling. To see this, we go back to the 2-level system described earlier. Let's assume the field is now on resonance but very weak. From Eq. 8 and 9 we see that the coupling $U^{-1}\frac{\partial}{\partial t}U \sim \dot{\theta} \propto \chi$, which is consistent with a π-pulse of duration $t = \pi/\chi$. In other words, while on resonance, no matter how small the coupling χ is, as long as we wait long enough, we can always have complete population transfer. The reason for this lies in the coupling phase – while off resonance, even though a large coupling amplitude induces a large transition rate, the wave function transfered at each time instance can add either constructively or destructively. While on resonance, all transfered wavefunction adds up in phase and therefore even a small coupling amplitude can move a large amount of population. In this aspect, the resonant transition is really a special case of non-adiabatic coupling. However, we will keep the distinction between these two mechanisms in the following discussion for two reasons: (1) Off-resonance non-adiabatic transitions are only noticeable when the coupling is strong, such as in SFI. In order to study this phenomenon, we should avoid any resonances. (2) Resonant transitions are often enabled by nuclear motion, and therefore offer a window on nuclear dynamics in the ion. In order to isolate resonance transitions driven by nuclear dynamics, we can work with sub 10 fs pulses, which effectively "freeze" out nuclear dynamics since the pulses are shorter than

the fastest vibrational period (C-H stretch at 11 fs).

II. EXPERIMENTS AND RESULTS

In the last section, we have seen that a resonance is a relationship between the energy gap and laser carrier frequency ($\Delta = \omega - (\omega_b - \omega_a)$), and the former depends on time indirectly via nuclear motion. On the other hand, non-adiabaticity depends on the energy gap (coupling phase) and the instantaneous field (coupling amplitude) independently. This implies that resonant transitions facilitated by nuclear dynamics prefer relatively long pulses since they allow more time for the nuclear wave packet to reach a resonance, while non-adiabatic transitions are mostly sensitive to the carrier frequency and the peak field strength of the pulse [17]. In order to compare these two effects, we carry out four coincidence VMI experiments measuring the indirect ionization yields, using 2 molecules (bromoiodomethane, CH_2BrI, and trifluoroiodomethane (CF_3I), and 10 and 30 fs pulses. We chose these two molecules because they have similar electronic structure (which has been studied in detail) with multiple low lying electronic states in the cation, but the former shows much more indirect ionization than the latter under similar experimental conditions [12].

The experimental apparatus is very similar to that used in previous work[18]. Briefly, our light source is an amplified Ti:sapphire laser system, producing 30 fs (intensity FWHM) pulses centered around 780 nm, at a 1 kHz repetition rate. We produce 10 fs pulses via filamentation-based spectral broadening and a grating-based pulse compressor [19]. The laser pulses are focused into an effusive molecular beam in a velocity map imaging (VMI) apparatus, which maps the transverse momentum of charged particles to spatial position on a dual stack microchannel plate (MCP) detector. A phosphor screen combined with a CMOS camera records the spatial distribution of particles [20]. A time-of-flight mass spectrum (TOFMS) is recorded by monitoring the voltage across the phosphor screen. Using the TOFMS information, we can identify the mass, and hence the species for each ion. When there is exactly one electron and one ion detected, it's considered a valid coincidence event. A detailed assessment of how false coincidences affect the measurement is provided in an earlier publication [12]. All electrons recorded have a partner ion, and they are grouped together to form the photoelectron spectra associated with the appropriate ion species. Since this experiment involves the comparison of two different molecules, the pulse intensity is chosen

to yield a similar ionization rate for all four measurments presented below.

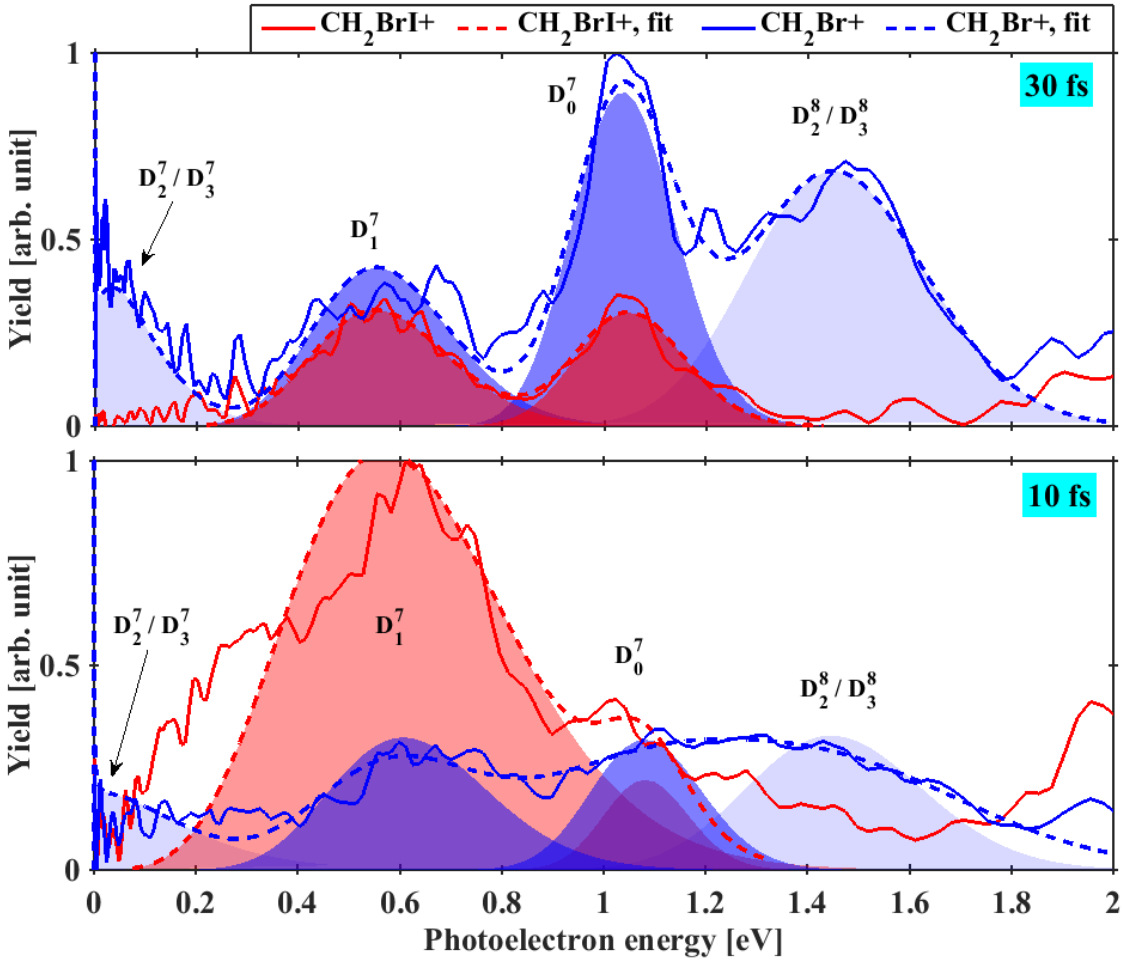

FIG. 2. Coincidence photoelectron spectra for CH_2BrI, with 30 fs (upper panel) and 10 fs (lower panel) pulses. Solid lines are measurements and dashed line are fits, which are the sums of all the shaded Gaussians of the respective color. Labels D_i^n denote electrons coming from the i^{th} order ionization to state D_i (see Equation 1).

Figure 2 and Figure 3 show photoelectron spectra measured in coincidence with photoions, for bromoiodomethane (CH_2BrI) and trifluoroiodomethane (CF_3I), respectively. The top panels are measured with 30 fs pulses and the bottom ones with 10 fs (The broadest spectrum produced by the filament supports 6 fs pulses. FROG measurements put an upper bound on the pulse duration of ∼10 fs.). Red (light grey) curves are the photoelectron spectra associated with the parent ion and the blue (dark grey) ones with the dominant fragment ion (For these two molecules, the parent and the chosen fragment account for more than

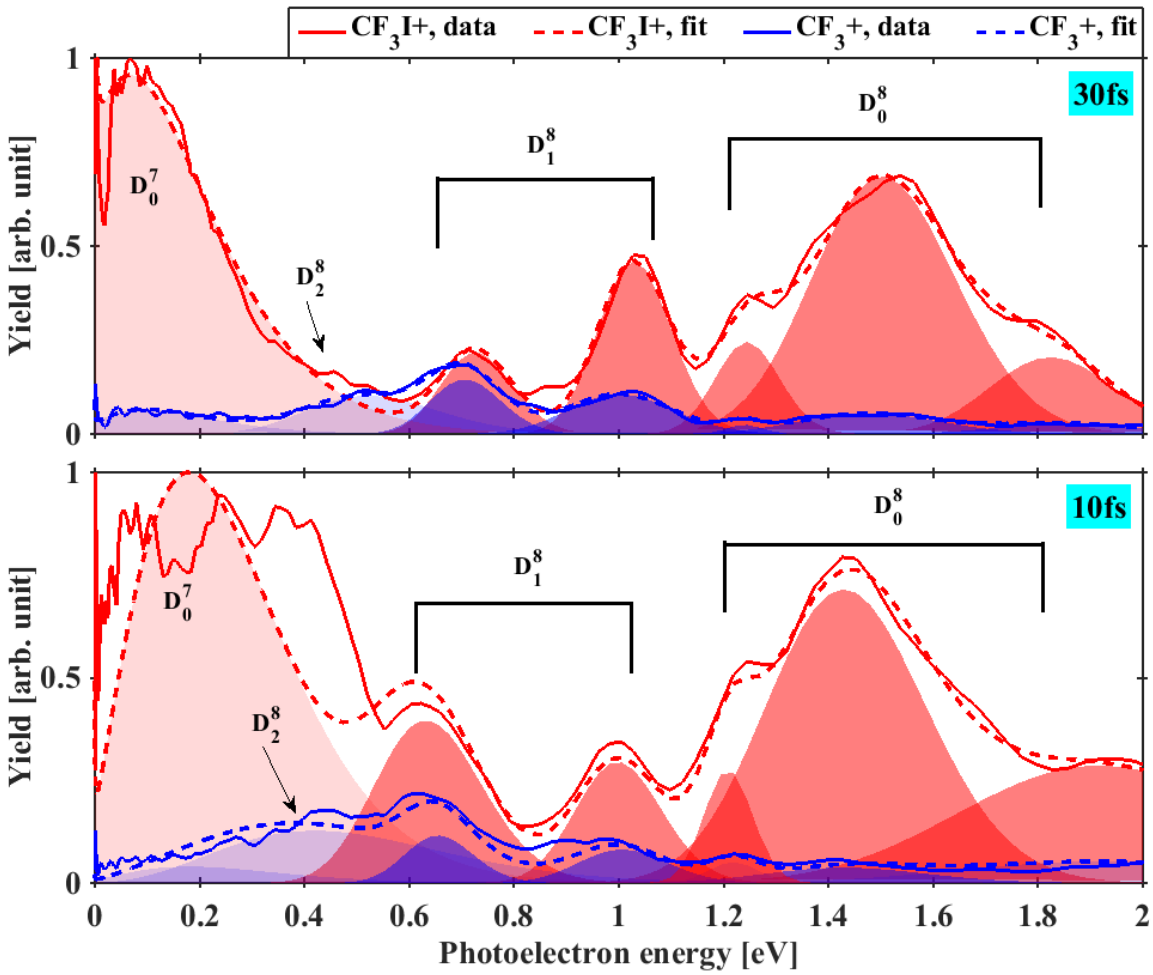

FIG. 3. Coincidence photoelectron spectra for CF_3I, with 30 fs (upper panel) and 10 fs (lower panel) pulses. Solid lines are measurements and dashed line are fits, which are the sums of all the shaded Gaussians of the respective color. Labels D_i^n denote electrons coming from the i^{th} order ionization to state D_i (see Equation 1). There are multiple peaks which are grouped to a single ionic state because while they correspond to the same ionic state, they correspond to different intermediate neutral states which Stark shift into resonance at different intensities and therefore lead to different ponderomotive shifts (cf equation 1).

90% of the yield in these experiments). Solid lines are measured data. Shaded areas are Gaussian fits whose sums are plotted as dashed lines. Given the ionization potentials of the relevant states (see Table I), coincidence detection allows us to assign various peaks in the spectra to states of the ion because of the relationship between the photoelectron energy and the ionization potential at the moment of ionization (see Equation 1). We refer interested

readers to previous work[18] for detailed methods used in assigning these peaks. Here we are mainly interested in the indirect ionization corresponding to those pairs of peaks at identical energies, one of which is measured in coincidence with the parent and the other with a fragment ion. The fact that these electrons have the same energy suggests that their cation partners are in the same state at the moment of ionization. However, after the electron is liberated, the cation is still subject to the laser field and can be excited to a more energetic dissociative state, producing fragment ions. The result is that some of these electrons are measured in coincidence with a fragment ion while the others with the parent. To better understand the underlying mechanism, we ask two questions: what percentage of the initially non-dissociative cations (D_0 and D_1 in our case) are field-excited to dissociative states, and how does the ratio vary with various parameters? To quantify our measurement, it's necessary to first fit the data.

TABLE I. Ionization potentials for CH_2BrI and CF_3I. D_0 denotes the ground ionic state and D_i denotes the i^{th} excited ionic state. "(d)" labels dissociative states.

Species	D_0(eV)	D_1(eV)	D_2(eV)	D_3(eV)
CH_2BrI [18]	9.69	10.26	10.91(d)	11.12(d)
CF_3I [21–23]	10.37	11.09	13.02(d)	15.17(d)

In order to fit the data, we start with a multi-Gaussian fit of the spectra in coincidence with the parent ion for 30 fs pulse. Then we fit the spectra associated with the fragment ion and impose the constraint that the indirect ionization peaks have the same centers and widths as their counterparts associated with the parent ion. Next, we fit the spectra taken with a 10 fs pulse. Generally speaking, the spectra may be shifted compared to those taken with 30 fs pulse since the central frequencies are not exactly the same. Since the optical spectrum is broader for a short pulse, we constrain the fitting to be no narrower than their counterparts for the 30 fs pulse. All measurements and fits are color-coded to distinguish between electrons in coincidence with parent and fragment ions. The sum of shaded areas gives the total fit plotted in dashed lines, which is to be compared with the measurement plotted in solid lines. We integrate each shaded Gaussian to calculate the yield associated with each pathway. Note that for CF_3I, we have named several peaks collectively D_0 or D_1 for they arise from multiple neutral resonant states with different Stark shifts [24] .

TABLE II. Ratio of non-dissociative states that undergo post-ionization excitation, which is calculated as $\frac{\text{dark blue area}}{\text{dark blue area + dark red area}} = \frac{\text{D}_0 \text{ (or D}_1\text{) peak in coincidence with fragment}}{\text{sum of two D}_0 \text{ (or D}_1\text{) peak}}$ in Figure 2 and 3. We estimate the errors in these ratios be about ±0.1, based on the background signal level.

	CH_2IBr		CF_3I	
	D_0^7	D_1^7	D_0^8	D_1^8
30 fs	0.67	0.50	0.05	0.22
10 fs	0.58	0.14	0.07	0.13

Table II lists the fractions of the molecules initially in non-dissociative ionic states that undergo post-ionization excitation to dissociative states. We note the following: (1) For CH_2IBr, the amount of indirect ionization generally decreases with pulse duration. This suggests that, under the conditions of our experiment, resonant transitions plays an important role. The amount of indirect ionization that persists in going from 30 fs to 10 fs could be due to two factors: First, since non-adiabatic transitions are less sensitive to pulse duration, it is likely the cause of the indirect ionization associated with D_1^7 for 10 fs pulses. Second, even though 10 fs pulses leave little time for nuclear dynamics, because of a broader range of available photon energies and a certain spatial spread of the nuclear wavepacket, it's still possible for some portion of the wavepacket to be in resonance if the resonance is close to the FC point. This should contribute to the indirect ionization associated with D_0^7 for 10 fs pulses. (2) In comparison, there is much less indirect ionization in CF_3I, regardless of the pulse duration. This suggests there is no resonant transition between D_0 or D_1 and higher lying dissociative states in the cation. (3) Note in Table I that the energy gaps between non-dissociative and dissociative states in CH_2IBr are smaller than our photon energy ($\sim$ 1.6 eV), as well as those in CF_3I. The smallest energy gap in CF_3I at the FC is between D_1 and D_2, and is about 2 eV. We will show in Sec. III that along the nuclear coordinate which largely describes the motion on D_0 and D_1 after ionization, there are 1-photon resonances in CH_2IBr near the FC while there is only one 2-photon resonance in CF_3I that is far away from the FC. We note that the relative change in the D_0 and D_1 yields with pulse duration is due to non-adiabatic dynamics in intermediate neutral states, which we considered in a separate study [25].

III. SIMULATIONS

In this section, we discuss two simulations. The first simulation models resonant transitions facilitated by nuclear dynamics in both CH_2BrI and CF_3I, and the second one explores the effects of non-adiabatic transitions.

All molecular parameters are obtained from *ab initio* electronic structure calculations. Geometry optimization of the parent CF_3I molecule and the CF_3I^+ cation in their ground electronic states are performed with time-dependent density functional theory (DFT) using the B3LYP functional [26, 27] and the aug-cc-pVTZ-PP basis [28] set with the help of the Gaussian09 program package [29]. Excited state energies of the cation at the Franck-Condon (FC) geometry and at the ground state minimum energy geometry (MIN) are computed with the multireference configuration interaction [30] method based on a state averaged complete active space self-consistent field (SA-CASSCF) [27] reference wavefunction using the Molpro program package [31]. Here the active space consists of 17 electrons distributed on 10 orbitals and 6 ^{2}A′, 6 ^{2}A", 1 ^{4}A′ and 2 ^{4}A" spin-free states are included in the averaging. For both the SA-CASSCF and MRCI computations on CF_3I^+, the Douglas-Kroll Hamiltonian and the ANO-RCC basis set [32, 33] are used, the latter with contractions [4s3p2d1f], [5s4p2d1f] and [7s6p4d2f1g] for carbon, fluorine and iodine atoms, respectively. Spin-orbit coupling was also taken into account in the final excited state energies. For simulating the dynamics in CH_2IBr^+, the molecular parameters (potential energy curves, spin-orbit couplings and transition-dipole moments) are taken from Ref. [34]. Previous simulations with these parameters are in excellent agreement with the results of pump-probe measurements.

For the first simulation (Figure 4), we solve the time-dependent Schrödinger equation (TDSE) at 51 fixed nuclear positions sampled uniformly between the FC and MIN geometry. The potential energies and transition dipole moments (TDM) at each nuclear position are linear interpolations of the values at FC and MIN. 8 ionic states for CH_2IBr and 10 for CF_3I are included in the TDSE. There are two non-dissociative states in each molecule (D_0 and D_1). We manually put a unity of population in a non-dissociative *dressed* state (D_0' or D_1') at the peak of the pulse and then solve the TDSE until the end of the pulse to calculate the fraction of the population that is excited to dissociative states (D_i, $i \geq 2$). Note that in the absence of the field, $D_i = D_i'$. The relative orientation of the TDMs with respect to the field polarization is taken into account by uniformly averaging the simulation

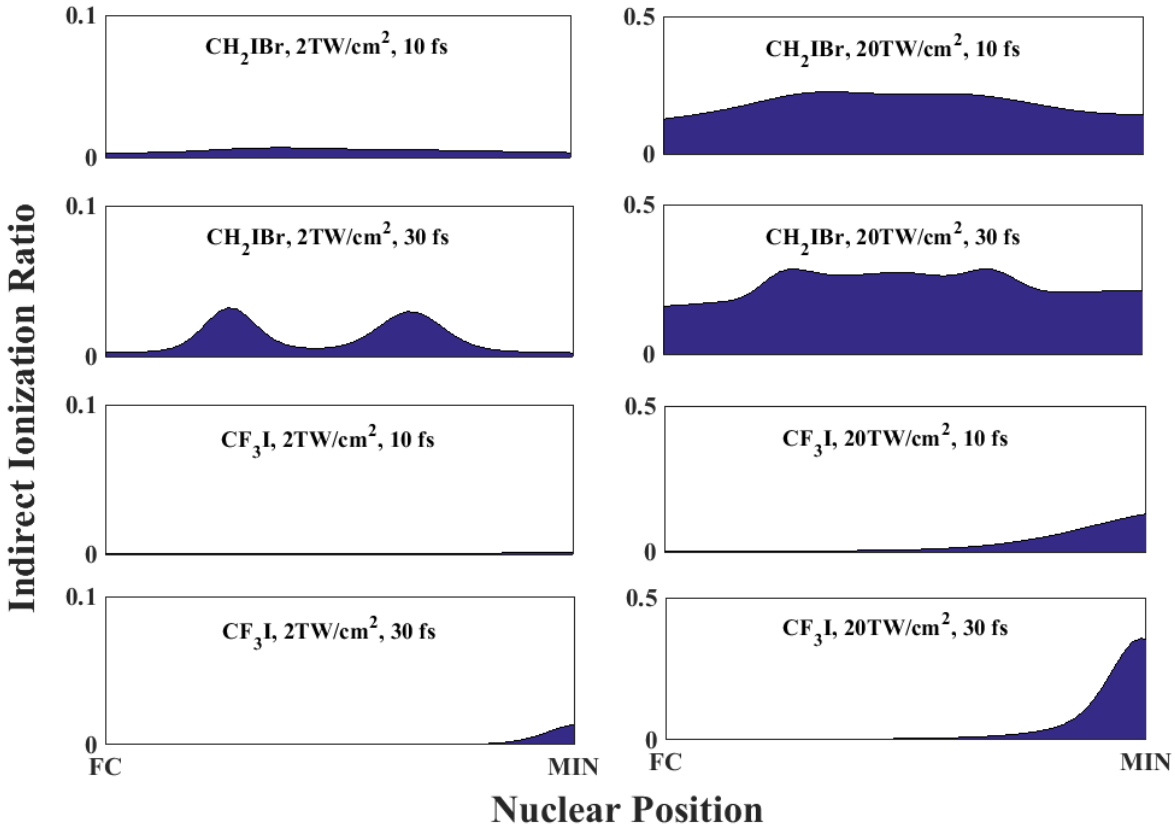

FIG. 4. Fractions of the initial ionic states populations (D_0 and D_1) excited to higher states as a function of nuclear coordinate between the FC point and the D_0/D_0 min for 10 and 30 fs pulses, and 2 and 20 TW/cm^2 peak intensities. 8 ionic states for CH_2IBr and 10 for CF_3I are included in the TDSE. There are 51 uniform sampling points between the Franck-Condon point and minimum of the potential. Each point is an average of contributions from both initial states and of 10 different orientations of the molecule with respect to the laser polarization. Note the difference in y-axis range for left and right columns.

results over 10 different angles.

As a separate check, we've solved the TDSE with nuclear dynamics included on a 3-state system (the ground neutral state, the ground ionic state and an excited ionic state). The system is modeled on CH_2BrI, that is, using the potential energy curves (PEC) and TDMs from the *ab initio* calculation. The simulation shows a similar result: significantly more population in $D_{2/3}$ with 30 fs pulse than that with 10 fs pulse. This approach is difficult to apply to CF_3I because, unlike in CH_2IBr, the dynamics in CF_3I don't occur along a single nuclear coordinate. So for simplicity, we only present the first approach here.

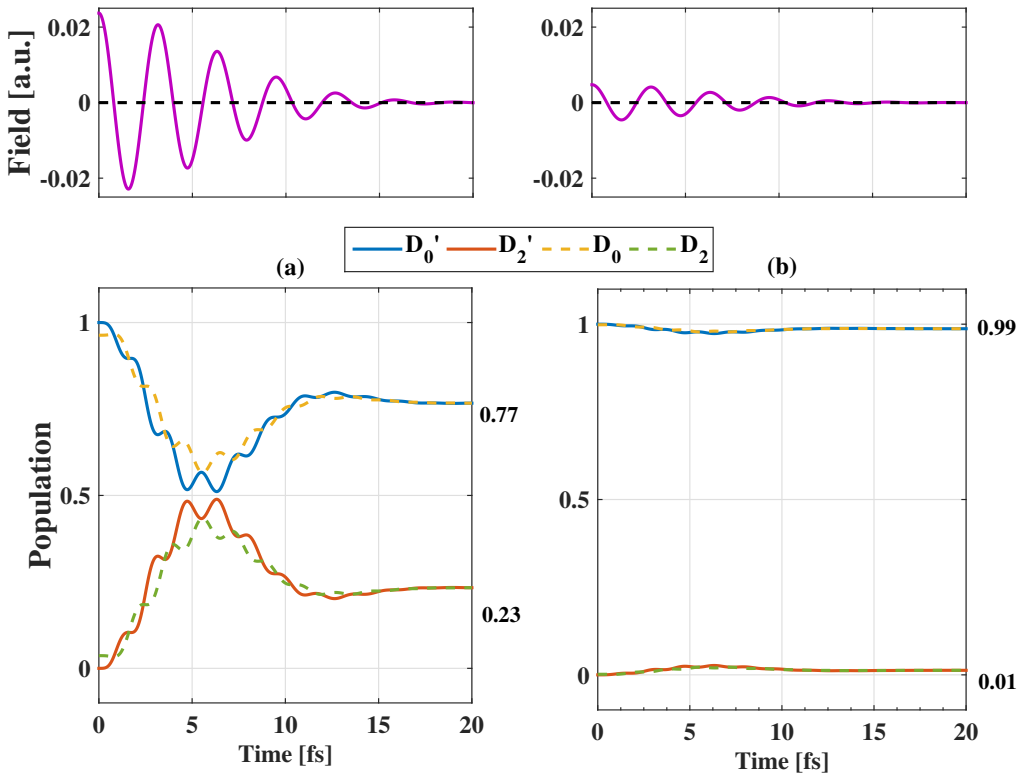

FIG. 5. *Dressed* and *bare* state populations during the laser pulse, for 20 TW/cm^2 (left panels) and 2 TW/cm^2 (right panels) peak intensities. All population starts from the *dressed* state D_0' at time t=0. The populations in these two states oscillate as the field goes to zero, at which point the *dressed* and *bare* states become identical. In the end, some population is left in D_2.

In Figure 4 , we plot the population percentage in dissociative states (starting with all the population in a non-dissociative state). As mentioned earlier, we see that there are two resonances in CH_2BrI which are closer to the FC point. The only resonance in CF_3I in this simulation comes at around the MIN point. At off-resonance locations, there is a lot more indirect ionization with 20 TW/cm^2 pulses than with 2 TW/cm^2, especially for CH_2IBr. The fact that there is less population transfer between ionic states in CF_3I than CH_2IBr results from a larger energy gap (see Table I) as well as weaker TDMs. Finally, we note that at the intensity closest to our experimental conditions ($10 \sim 20$ TW/cm^2), the amount of indirect ionization in both molecules is in qualitative agreement with our measured results.

In order to better understand the effect of non-adiabatic transitions, we consider a 2-

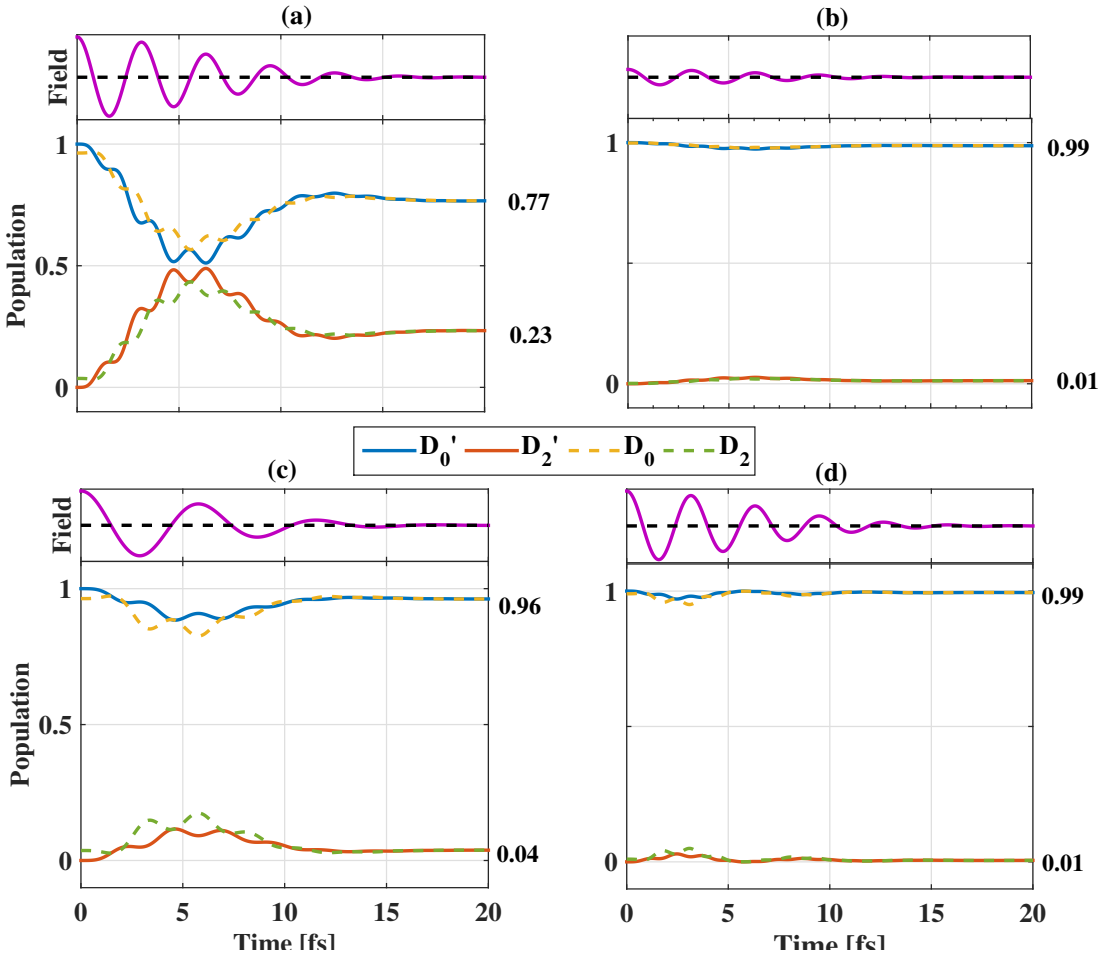

FIG. 6. *Dressed* and *bare* state populations during the laser pulse. A unit population is put into the *dressed* state D_0' by hand at time t=0. The populations oscillate as the field goes to zero, at which point the *dressed* and *bare* states become identical. In the end, some population is left in the second *bare* state, D_2. (a) 20 TW/cm^2 peak intensity, 1 eV energy gap, 1.3 eV photon energy. (b) 2 TW/cm^2 peak intensity, 1 eV energy gap, 1.3 eV photon energy. (c) 20 TW/cm^2 peak intensity, 1 eV energy gap, 0.7 eV photon energy. (d) 20 TW/cm^2 peak intensity, 2 eV energy gap, 1.3 eV photon energy.

level system in a laser field, (Fig. 5). The TDMs used here are borrowed from the *ab initio* calculation in CH_2IBr, while we set the pulse peak intensity to either 20 TW/cm^2 (left panels) and 2 TW/cm^2 (right panels). We assume ionization via tunneling at the peak of the pulse by manually putting all the population in the *dressed* state D_0' at t=0. Then we solve the TDSE and see how the populations in both *dressed* and *bare* states change as the field turns off. Were the adiabatic approximation valid, we would expect the

population to remain in the lower *dressed* state D_0' the whole time as the field oscillates to zero. As the *dressed* and *bare* states coincide in the absence of the field, this implies that the system would have been in the ground ionic state at the end of the pulse. This is the case for the lower intensity (2 TW/cm^2), while in the case of the 20 TW/cm^2 pulse we see significant non-adiabatic dynamics. The missing population in D_0' can be seen as the non-adiabatic response of the system to the applied field. We also studied the dependence of non-adiabatic transitions on the carrier frequency and gap energy. These are illustrated in figure 6, which shows the dependence of non-adiabatic transitions on pulse intensity (panel (a) vs (b)), carrier frequency (panel (a) vs (c)) and gap energy (panel (a) vs (d)). These results corroborate the expectations described in the analytic treatment above.

IV. CONCLUSION

Coincidence detection of electrons and ions provide a means to discriminate between direct and indirect ionization. In order to understand the mechanism underlying indirect ionization, we measured photoelectron spectra in coincidence with molecular cations for two molecules in the halomethane family with 10 and 30 fs pulses. We see more indirect ionization when there are resonant transitions, consistent with our simulations. The simulations which consider non-adiabatic transitions illustrate the dependence on pulse intensity, carrier frequency and gap energy. They also suggest an increasingly important role of off-resonance non-adiabatic transitions as one goes to more intense laser fields. Although the experimental data is consistent with a small amount of non-adiabatic indirect ionization, a more targeted experiment is needed to quantify this effect at higher intensities.

ACKNOWLEDGMENTS

We would like to thank Ludwig Krinner for insightful discussions. This work has been supported by the National Science Foundation under award number 1205397. Support from the European XLIC COST Action CM1204 is also acknowledged.

Appendix A: Definition of U Matrix

Let $U(t)$ be the unitary transformation that diagonalizes the instantaneous Hamiltonian $H(t)$. One can show [35] that for a 2-level system :

$$U(t) = \begin{pmatrix} \cos(\frac{\theta}{2})e^{-i\phi/2} & -\sin(\frac{\theta}{2})e^{-i\phi/2} \\ \sin(\frac{\theta}{2})e^{+i\phi/2} & \cos(\frac{\theta}{2})e^{+i\phi/2} \end{pmatrix} \tag{A1}$$

where

$$E'_{a/b} = \frac{1}{2}(E_a + E_b) \pm \frac{1}{2}\sqrt{(E_a - E_b)^2 + 4V^2} \tag{A2}$$

$$\tan\theta = \frac{2|V|}{E}, \quad E = E_a - E_b \equiv \hbar\omega_0 \tag{A3}$$

$$V = |V|e^{i\phi} \tag{A4}$$

Since we've assumed $V = V^*$, hence $\phi = 0$ and the TDSE in the *dressed* state basis becomes:

$$i\hbar\frac{\mathrm{d}}{\mathrm{d}t}\begin{pmatrix} a'(t)e^{-i\omega'_a t} \\ b'(t)e^{-i\omega'_b t} \end{pmatrix} = \begin{pmatrix} E'_a & \frac{i\hbar\dot{\theta}}{2} \\ -\frac{i\hbar\dot{\theta}}{2} & E'_b \end{pmatrix}\begin{pmatrix} a'(t)e^{-i\omega'_a t} \\ b'(t)e^{-i\omega'_b t} \end{pmatrix} \tag{A5}$$

which simplifies to Equation 10

Appendix B: Simulation Model

A strong IR pulse couples ionic states

$$E_{IR} = \mathcal{E}_{IR}(t)\frac{(e^{i\omega_{IR}t} + c.c.)}{2} \tag{B1}$$

where $\mathcal{E}(t) = \mathcal{E}e^{-\frac{t^2}{2T^2}}$ is a Gaussian temporal envelope with intensity FWHM $= 2\sqrt{ln2}\ T$, which is set to 10 or 30 fs in the current case.

The molecular system consists of several ionic states, whose energies and transition dipole moments are obtained from *ab initio* electronic structure calculation. The total electronic Hamiltonian consists of the free Hamiltonian H_0 and the molecule-field dipole-coupling H_{MF}:

$$H = H_0 + H_{MF} \tag{B2}$$

$$H_{MF} = -\vec{\mu} \cdot \vec{E} \tag{B3}$$

$$H_0 \left|\phi_i\right\rangle = \hbar\omega_i \left|\phi_i\right\rangle \tag{B4}$$

$$\left|\psi(t)\right\rangle = \sum_i \tilde{a_i}(t) \left|\phi_i\right\rangle \tag{B5}$$

Substituting (B2) and (B5) into the time dependent Schrödinger equation $i\hbar\frac{\partial}{\partial t}\left|\psi\right\rangle = H\left|\psi\right\rangle$ and transforming into the rotating frame $\tilde{a}_i(t) = a_i(t)e^{-i\omega_i t}$, we arrive at :

$$\dot{a}_i = \frac{i}{\hbar}\sum_{j\neq i} \mu_{ij} 2\mathcal{E}_{IR}(t) cos(\omega_{IR}t) a_j(t) e^{-i\omega_{ji}t} \tag{B6}$$
$$\omega_{ij} = \omega_i - \omega_j$$

We take into account the dependence of both H_0 and $\vec{\mu}$ on nuclear position by uniformly sampling between the Franck-Condon point and minimal potential point. The orientation of the molecule is accounted for by averaging 10 different orientations of the $\vec{\mu}$ with respect to $\vec{E}$. Solving Equation B6 gives us Figure 4.

REFERENCE

[1] P. Agostini and L. F. DiMauro, Reports on progress in physics **67**, 813 (2004).

[2] M. F. Kling and M. J. Vrakking, Annu. Rev. Phys. Chem. **59**, 463 (2008).

[3] F. Krausz and M. Ivanov, Reviews of Modern Physics **81**, 163 (2009).

[4] W. Li, A. A. Jaroń-Becker, C. W. Hogle, V. Sharma, X. Zhou, A. Becker, H. C. Kapteyn, and M. M. Murnane, Proceedings of the National Academy of Sciences **107**, 20219 (2010).

[5] G. Gibson, R. Freeman, and T. McIlrath, Physical Review Letters **67**, 1230 (1991).

[6] H. Akagi, T. Otobe, A. Staudte, A. Shiner, F. Turner, R. Dörner, D. Villeneuve, and P. Corkum, Science **325**, 1364 (2009).

[7] A. E. Boguslavskiy, J. Mikosch, A. Gijsbertsen, M. Spanner, S. Patchkovskii, N. Gador, M. J. Vrakking, and A. Stolow, Science **335**, 1336 (2012).

[8] M. Kotur, C. Zhou, S. Matsika, S. Patchkovskii, M. Spanner, and T. C. Weinacht, Physical Review Letters **109**, 203007 (2012).

[9] W. Li, X. Zhou, R. Lock, S. Patchkovskii, A. Stolow, H. C. Kapteyn, and M. M. Murnane, Science **322**, 1207 (2008).

[10] H. Liu, S.-F. Zhao, M. Li, Y. Deng, C. Wu, X.-X. Zhou, Q. Gong, and Y. Liu, Physical Review A **88**, 061401 (2013).

[11] B. K. McFarland, J. P. Farrell, P. H. Bucksbaum, and M. Ghr, Science **322**, 1232 (2008).

[12] A. Zhao, P. Sándor, T. Rozgonyi, and T. Weinacht, Journal of Physics B: Atomic, Molecular and Optical Physics **47**, 204023 (2014).

[13] M. Spanner, S. Patchkovskii, C. Zhou, S. Matsika, M. Kotur, and T. C. Weinacht, Physical Review A **86**, 053406 (2012).

[14] I. Znakovskaya, P. von den Hoff, S. Zherebtsov, A. Wirth, O. Herrwerth, M. J. J. Vrakking, R. de Vivie-Riedle, and M. F. Kling, Physical review letters **103**, 103002 (2009).

[15] I. Znakovskaya, P. von den Hoff, N. Schirmel, G. Urbasch, S. Zherebtsov, B. Bergues, R. de Vivie-Riedle, K.-M. Weitzel, and M. F. Kling, Physical Chemistry Chemical Physics **13**, 8653 (2011).

[16] M. Lezius, V. Blanchet, M. Y. Ivanov, and A. Stolow, The Journal of Chemical Physics **117**,

1575 (2002).

[17] The time variation of the intensity envelope will be important only when the pulse is very short, that is, the time scale of the change in the intensity envelope is comparable to the period of the carrier.

[18] P. Sándor, A. Zhao, T. Rozgonyi, and T. Weinacht, Journal of Physics B: Atomic, Molecular and Optical Physics **47**, 124021 (2014).

[19] G. Stibenz, N. Zhavoronkov, and G. Steinmeyer, Opt. Lett. **31**, 274 (2006).

[20] A. T. J. B. Eppink and D. H. Parker, Review of Scientific Instruments **68**, 3477 (1997).

[21] N. Macleod, S. Wang, J. Hennessy, T. Ridley, K. Lawley, and R. Donovan, Journal of the Chemical Society. Faraday transactions **94**, 2689 (1998).

[22] L. D. Waits, R. J. Horwitz, R. G. Daniel, J. A. Guest, and J. R. Appling, The Journal of Chemical Physics **97** (1992).

[23] F. Aguirre and S. T. Pratt, The Journal of Chemical Physics **119** (2003).

[24] W. D. Lunden, D. Geißler, P. Sándor, T. C. Weinacht, and T. Rozgonyi, Physical Review A **89**, 053404 (2014).

[25] P. Sándor, V. Tagliamonti, A. Zhao, T. Rozgonyi, M. Ruckenbauer, P. Marquetand, and T. Weinacht, Physical Review Letters **116**, 063002 (2016).

[26] C. Lee, W. Yang, and R. G. Parr, Physical Review B **37**, 785 (1988).

[27] B. O. Roos, P. R. Taylor, P. E. Si, *et al.*, Chemical Physics **48**, 157 (1980).

[28] K. A. Peterson, The Journal of Chemical Physics **119**, 11099 (2003).

[29] M. Frisch, G. Trucks, H. Schlegel, G. Scuseria, M. Robb, J. Cheeseman, G. Scalmani, V. Barone, B. Mennucci, G. Petersson, *et al.*, "Gaussian 09, revision d. 01," (2009).

[30] P. J. Knowles and H.-J. Werner, Theoretical Chemistry Accounts: Theory, Computation, and Modeling (Theoretica Chimica Acta) **84**, 95 (1992).

[31] H. Werner, P. Knowles, G. Knizia, F. Manby, M. Schütz, P. Celani, T. Korona, R. Lindh, A. Mitrushenkov, G. Rauhut, *et al.*, "Molpro, version 2012.1, a package of ab initio programs, cardiff, uk," (2012).

[32] P.-O. Widmark, P.-Å. Malmqvist, and B. O. Roos, Theoretical Chemistry Accounts: Theory, Computation, and Modeling (Theoretica Chimica Acta) **77**, 291 (1990).

[33] B. O. Roos, R. Lindh, P.-Å. Malmqvist, V. Veryazov, and P.-O. Widmark, The Journal of Physical Chemistry A **108**, 2851 (2004).

[34] J. González-Vázquez, L. González, S. R. Nichols, T. C. Weinacht, and T. Rozgonyi, Physical Chemistry Chemical Physics **12**, 14203 (2010).

[35] D. J. Tannor, *Introduction to quantum mechanics: a time-dependent perspective* (University Science Books, 2007).